Environ Monit Assess (2024) 196:96
https://doi.org/10.1007/s10661-023-12246-x

RESEARCH

Characterization of clay and nanoclay extracted from a semi-arid Vertisol and investigation of their carbon sequestration potential

Niloofar Sadri · Majid Baghernejad · Reza Ghasemi-Fasaei · Ali Akbar Moosavi · Ailsa G. Hardie

Received: 23 October 2023 / Accepted: 14 December 2023 / Published online: 28 December 2023

Abstract Mitigation of global climate change by means such as soil carbon (C) sequestration has become an important area of research. Soil organic matter (SOM) that is stabilized with clay minerals is the most persistent in soils. Currently, little is known regarding the C sequestration ability of nanoclay extracted from Vertisols in semi-arid regions. Therefore, the aim of this study was to extract and characterize nanoclay and bulk clay from a Vertisol from Iran, in terms of physicochemical surface properties and resistance of SOM to chemical oxidation. The clay fractions were studied before and after H_2O_2 treatment by total C analysis, scanning electron microscopy (SEM), transmission electron microscopy (TEM), dynamic light scattering (DLS), pyrolysis gas chromatography mass spectrometry (GC–MS), Fourier transform infrared (FTIR) spectroscopy, specific surface area analysis, and zeta potential. TEM and SEM images showed that the diameter of the extracted nanoclays was 16–46 nm and their morphology was more porous than bulk soil clay. The nanoclay had a much greater specific surface area (111.9 $m^2\ g^{-1}$) than the bulk clay (67.9 $m^2\ g^{-1}$). According to total C, FTIR, and zeta potential results, the nanoclay was enriched with 1.4 times more C than the bulk clay after peroxide treatment, indicating enhanced soil C stabilization in the nanoclay. About 45% of the peroxide-resistant SOM in the nanoclay was associated with N-containing compounds, indicating that these compounds contribute to SOM stability. The results demonstrate important role of nanoclay in soil C sequestration in Vertisols.

Keywords Nanotechnology · Soil organic carbon stabilization · Soil organic matter,·2:1 clays,·Zeta potential

Introduction

Global progressive industrialization and urbanization has resulted in substantial harmful environmental effects that threaten the sustainability of humanity. The combustion of fossil fuels and wide-spread deforestation have exponentially increased the emissions of carbon dioxide (CO_2) into the atmosphere in the past century (Kumar et al., 2020). Loss of soil organic carbon (SOC) due to modern agricultural practices such as tillage is another major source of atmospheric CO_2 (Lal et al., 2015). Increasing atmospheric concentrations of CO_2 results in global warming and associated climate change; thus, it is imperative to take

N. Sadri (✉) · M. Baghernejad · R. Ghasemi-Fasaei · A. A. Moosavi
Department of Soil Science, School of Agriculture, Shiraz University, Shiraz, Iran
e-mail: niloofar.sadri91@gmail.com

A. G. Hardie
Department of Soil Science, University of Stellenbosch, Private Bag X1, Stellenbosch 7600, South Africa

necessary measures to reduce CO_2 in the atmosphere (Ghosh et al., 2023).

In the global carbon (C) cycle, soil is considered a major source and sink of atmospheric C, and able to absorb 20% of anthropogenic C emissions (Minasny et al., 2017; Powlson et al., 2011; Yang et al., 2021). Soil C sequestration is not only important for reducing greenhouse gases and mitigating climate change (Churchman et al., 2020; Paustian et al., 2019), but also plays a key role in improving fertility, soil health, and the sustainability of agriculture (Lal et al., 2015).

As an abundant adsorbent in nature, clay is the most reactive soil fraction in stabilizing organic matter and plays a central role in SOC sequestration (Singh et al., 2018). Recent studies show that up to 90% of soil organic matter (SOM) is associated with soil minerals and that this mineral-associated organic C fraction is the most persistent in soils (Ahmat et al., 2017; Chen et al., 2018; Cortrufo & Lavallee, 2022; Schrumpf et al., 2013). Many researchers suggest that SOC can be stabilized by binding to clay mineral surfaces or being trapped between microaggregates (Angst et al., 2017; Cortrufo & Lavallee, 2022; Lützow et al., 2006; Zayed et al., 2018). Clay minerals can chemically bind with SOM through ligand exchange, polyvalent cation bridging, electrostatic attraction, H-bonding, and van der Waals forces (Sarkar et al., 2018; Singh et al., 2018). Much of the SOM is trapped between the clay layers, and therefore soils dominated by 2:1 layer silicate clay minerals, especially smectites, sequester C more efficiently than those dominated by 1:1 minerals (Churchman et al., 2020; Feng et al., 2013; Six et al., 2002).

Nanoclays (diameter < 100 nm) are much more reactive than larger clay particles due to their higher specific surface area, surface charge density and reactivity, and porosity (Calabi-Floody et al., 2009, 2011; Pramanik et al., 2020). Nanoclay fractions are the preferred sites for the accumulation of stabilized SOM (Calabi-Floody et al., 2011, 2015; Monreal et al., 2010). Monreal et al. (2010) examined the nature and stability of C associated with nanoclay and clay from a cultivated Canadian Chernozem (mainly 2:1 layer silicate clays). They observed a greater thermal and chemical stability of C associated with nanoclays than soil clays. Calabi-Floody et al. (2015) examined the C sequestration ability of nanoclay extracted from an Andisol (mainly allophane) and Cambisol (mainly kaolinite). They found that the Andisol nanoclay sequestered and stabilized C to a much greater extent than the Cambisol nanoclay due to differences in clay mineralogy.

Vertisols occupy approximately 2.3 to 2.8% of the world's land area, with 30% and 60% of them located in subtropical and tropical regions, respectively (Blum & Eswaran, 2004; Coulombe et al., 1996; Pal et al., 2012). Vertisols are very fertile and have a high clay content of the smectite type (Najafi Ghiri & Abtahi, 2011). About 70,000 ha of agricultural land in Iran consists of Vertisols, mostly located in the four provinces of Fars, Kermanshah, Lorestan, and Ardabil (Heidari & Mahmoodi, 2005). As Vertisols are important soils for agricultural production in semi-arid regions, it is critical to investigate the mechanisms of clay mineral SOC stabilization. There is currently little information about the role of nanoclay from Vertisols in SOC sequestration. Therefore, the objectives of the present study were (i) to evaluate the capacity of extracted clay and nanoclay to sequester C in Vertisols using chemical oxidation (H_2O_2) treatment and (ii) to characterize the physicochemical properties of clay and nanoclay before and after H_2O_2 treatment.

Materials and methods

Soil sample collection and clay extraction

Based on the previous studies of the distribution of Vertisols in Fars province, the Vertisols of Sepidan region, southern Iran (30° 16′N 51° 59′E), were chosen as a representative of the Vertisols in Fars province, due to their typical vertic characteristics and high clay content (51%) (Najafi Ghiri & Abtahi, 2011). Three soil samples from the mentioned Vertisols of Sepidan region were collected from a surface horizon (0–30 cm). The selected soils were classified as fine, smectitic, mesic, Typic Haploxererts. Soils were air-dried and passed through a 2-mm sieve prior to analysis. The characteristics of the selected soils determined using the standard methods. Soil particle size analysis was determined by method of Rowell (1994). The cation exchange capacity (CEC) was measured by using sodium acetate at pH 8.2 (Chapman, 1965). Soil organic C (SOC) was determined by wet oxidation with chromic acid followed by titration using ferrous ammonium sulfate (Nelson & Sommers,

1982). Calcium carbonate equivalent (CCE) was determined by a titration process (Salinity Laboratory Staff, 1954). Soil pH in soil saturated paste and electrical conductivity (EC) in soil saturated extract was determined using glass-electrode pH-meter and EC-meter, respectively (Salinity Laboratory Staff, 1954). The characteristics of the selected soils are shown in Table 1.

Extraction of clays was carried out using the procedure proposed by Calabi-Floody et al. (2015). To separate the clay fraction, 180 ml of deionized water was added to 50 g of the soil samples, and the samples were shaken overnight. Particles with size less than 50 µm were separated by a wet sieve. The soil suspension was dispersed by probe sonication (SONOPULS HD-4200, Germany) by applying 150 kW s^{-1}. The soil suspension was then placed in 1-l cylinders and the clay fraction (less than 2 µm) of the soil was separated based on Stokes' law (Eq. 1), where v is the velocity of a particle falling in a liquid (cm s^{-1}), g is the acceleration of gravity (cm s^2), r is the particle radius (cm), p_P is the particle density (g cm^{-3}), p_F is the fluid density (g cm^{-3}), and $\eta$is the fluid viscosity (g cm^{-1} s^{-1}). The suspension was then dried at 60 °C.

$$v = \frac{2\,g\,r^2\left(p_P\text{-}p_F\right)}{9\eta} \tag{1}$$

Nanoclay extraction

Nanoclays were extracted from the clay fraction using the method of Calabi-Floody et al. (2015). In short, 5 g of bulk clay was dissolved in 1 M NaCl solution and sonicated for 3 min at a power of 21.4 kJ and then centrifuged (Hermle Z446) to separate the nanoclay. The time required for the sedimentation of a given diameter of particles under centrifugal acceleration was calculated based on the below equation (Eq. 2) where time in minutes is shown as t_{min}, N_m is the rotor speed in rpm, R is the radius of rotation of the upper part of the sediment in the tube (cm), S is the radius of rotation of the surface of the suspension in the tube (cm), $D_{\mu m}$ is the particle diameter in micrometers, and ΔS is the contrast between the dissolved particles and the suspension fluid expressed as specific gravity. (R/S) was estimated to be 7 mm, considering the speed driven in the angular centrifuge (Paul et al., 2017). The time required to separate nanoparticles less than 100 nm was calculated to be 4 min at 6000 rpm under the conditions of the experiments. In the first round of centrifugation the supernatant was separated, and after the second round of centrifugation, the supernatant containing the nanoclay was collected.

$$t_{min}=\frac{63.0\times10^8\ \eta\ \log^{10}\left(\frac{R}{S}\right)}{(N_m)^2\left(D_{\mu m}\right)^2(\Delta S)} \tag{2}$$

Organic C oxidation treatment

An aliquot of the clay and nanoclay in three replicates were treated with 30% hydrogen peroxide (H_2O_2) to oxidize the organic matter. The suspended clays were first acidified to pH 2.0 with 0.1 M HCl. The H_2O_2 was then added to soil at a ratio of 1:2 H_2O_2 to acidified clay suspension, and then heated at 60 °C with stirring for 16 h. After peroxidation, 0.1 M NaOH was used to neutralize the suspensions and the excess peroxide was removed using dialysis (1000 kDa membrane tubing) in deionized water (Calabi-Floody et al., 2011).

X-ray diffraction (XRD)

For layer silicate mineralogical identification, the clay fraction was extracted and pre-treated to remove organic matter and free iron oxides according to the method of Mehra and Jackson (1958). Aliquots of the pre-treated clay were then saturated with Mg^{2+} and K^+ as described in the standard procedure for soil

Table 1 Selected chemical and physical characteristics of the studied Vertisol A horizon (0–30 cm) (*EC*, electrical conductivity; *CEC*, cation exchange capacity; *SOC*, soil organic carbon; *CCE*, calcium carbonate equivalent)

pH (1:2)	EC (dS m^{-1})	SOC (%)	CCE (%)	CEC $cmol_{(+)}$ kg^{-1}	Texture class	Clay (%)	Silt (%)	Sand (%)
7.3	0.4	1.2	3	34	Clay	51	36	13

clay mineral identification by Whittig and Allardice (1986). The Mg-saturated clay sample was analyzed before and after treatment with the solvent ethylene glycol in order to identify smectites. The K-saturated sample was analyzed before and after heating to 550 °C in order to identify kaolinite. The radiation type was CuKa (λ = 1.5418 Å), voltage 40 kV, tube current 30 mA, and 2 theta in the range 2–80°. Mineralogical identification of the bulk clay fractions was determined using X-ray diffraction (XRD) with a Philips Pw 1130/00 diffractometer (Phillips, Netherlands). Semi-quantification of the identified minerals in the diffractograms was performed using UPEX software (Mehrabadi & Faghihian, 2018).

Transmission electron microscopy (TEM)

Transmission electron microscopic (TEM) images were taken to determine the size of clay and nanoclay and to confirm the presence of nanoclay. Firstly, the clay and nanoclay were suspended in deionized water and then 10 µL of the suspensions was placed on a copper grid covered with a thin carbon film and allowed to dry. The TEM images were then taken with a (Philips 906E instrument, Germany) operating at a voltage of 120 kV.

Surface area and porosity analysis

N_2 adsorption and desorption isotherms of the clay and nanoclay samples were performed at 77 K and liquid nitrogen at − 196 °C with a BELSORP MINI II (Verder Scientific, Germany) surface area and pore size distribution analyzer. Prior to measurement, samples were degassed for 2 h at 120 °C with a BELPREP VAC II (Verder Scientific, Germany). Specific surface area and mean particle diameter of clay and nanoclay were calculated using BET and Barrett-Joyner-Halenda (BJH) methods, respectively (Barrett et al., 1951; Brunauer et al., 1938).

Total C content and pyrolysis-mass spectrometry

The total C content in the clay and nanoclay fractions was determined in three replicates by dry combustion with a (SERIES II 2400 analyzer, PERKINELMER, USA). Molecular composition of SOM associated with clay and nanoclay was performed using a gas chromatography/mass selective detector (GC/MSD) Agilent 7890B [split injector, 250 °C; flame ionization detector (FID) at 300 °C] (Agilent Technologies, USA). First, clay and nanoclay samples before and after H_2O_2 treatment dissolved in ethanol were entered into the device. The products are then separated using a fused silica column (HP-5, 30 m × 0.32 mm × 0.25 µm (19091J-413)). The initial temperature (75 °C) of the GC oven was raised to 280 °C at a rate of 3 °C min^{-1}.

Fourier Transform Infrared (FTIR) spectroscopy

FTIR spectra of the extracted clay and nanoclay before and after H_2O_2 treatment were performed on attenuated total reflectance (ATR)-FTIR spectrometer (Tensor II Bruker, Germany) to confirm the presence of functional groups. The samples were scanned between 400 and 4000 cm^{-1}.

Scanning electron microscopy (SEM)

For the scanning electron microscopy (SEM) study, clay and nanoclay were sonicated at 150 kW for 5 min before and after H_2O_2 treatment. Ten microliters of the sonicated suspension was then applied to a freshly cleaned silicon wafer and allowed to evaporate near the Petri dish under ambient conditions. Scanning electron microscope (TESCAN-Vega 3, Czech Republic) at 20.0 kV and high torque vacuum was used to obtain SEM images of the clay samples.

Electrophoretic mobility and dynamic light scattering (DLS) measurements

Zeta potentials of the clays were measured at pH values of 2, 4, 6, and 8, which were obtained by adjustment of the solution with 0.01 M HCl and NaOH. Briefly, 1 mg of extracted clay and nanoclay, before and after H_2O_2 treatment, was dispersed in 0.001 M NaCl in an ultrasonic bath. Subsequently, the average diameter and zeta potential of the clay and nanoclay particles were measured using a HORIBA-SZ-100 (Japan) apparatus.

Statistical analysis

A comparison of the C sequestration potential of bulk clay and nanoclay was tested. Analysis of variance (ANOVA) was performed using SPSS ver. 16.0

(SPSS Inc., Chicago, IL, USA). A mean comparison test was performed at a 0.05 significant probability level using Duncan's method through SPSS ver. 16.0.

Results and discussion

Soil chemical, physical, and mineralogical characteristics

The soil chemical and physical properties are shown in Table 1. The clay-textured soil (51% clay) had a slightly alkaline pH (7.3), and CCE of 3%. The SOC and CEC were 1.2% and 34 $cmol_{(+)}\ kg^{-1}$, respectively (Najafi Ghiri & Abtahi, 2011).

The X-ray diffractograms of the extracted bulk clay fraction is shown in Fig. 1. The peak at 1.8 nm of the Mg-saturated ethylene glycol treated sample compared to the Mg treatment indicates the presence of swelling smectite minerals (Whittig & Allardice, 1986). The presence of illite in all treatments (Mg, Mg-saturated ethylene glycol, K, K-heat at 550 °C) was indicated by a peak at 1 nm. The disappearance of the peak at 0.7 nm in the K-saturated treatment heated to 550 °C indicates the presence of kaolinite in the soil (Whittig & Allardice, 1986). The bulk extracted clay fraction of the soil was estimated to be composed predominantly of smectite (50%), with some kaolinite and illite (21%) also present. In general, about 67% of the minerals in Vertisols are related to 2:1 smectite minerals (Das et al., 2022). Smectite was also found to be the dominant mineral in Indian Vertisols (Paul et al., 2021).

Transmission electron microscopy (TEM)

The transmission electron microscope (TEM) patterns revealed that the bulk extracted clay particles had a rounded edge morphology (Fig. 2A). According to the images obtained by TEM, the clay particles had bent layers with thin edges, some were flat amorphous crystals and some had rounded edges (Fesharaki et al., 2007). However, nanoclay extracted from the Vertisol consisted primarily of grains that were coarse in the middle and smooth at the edges (Fig. 2B, C, D) (Carbajal de la Torre et al., 1998). Particle size analysis of the TEM images of the nanoclay showed that the nanoparticle size ranged from 16 to 46 nm, which is similar to the dimensions reported for montmorillonite nanoclay (22–45 nm) separated from bentonite (Atigh et al., 2021).

Dynamic light scattering (DLS) particle size analysis

Approximately 90% of the nanoclay separated from the soil was 38.8 nm in size (Fig. 3), which confirms

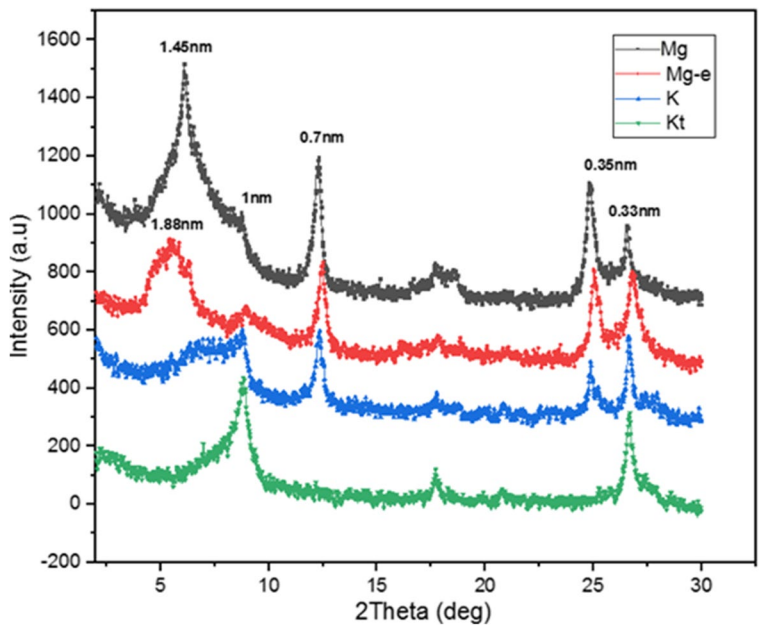

Fig. 1 X-Ray diffractograms of the extracted bulk clay (Mg-saturated (Mg); Mg-saturated with ethylene glycol treatment (Mg-e); K-saturated (K); K-saturated with heating treatment at 550 °C (Kt))

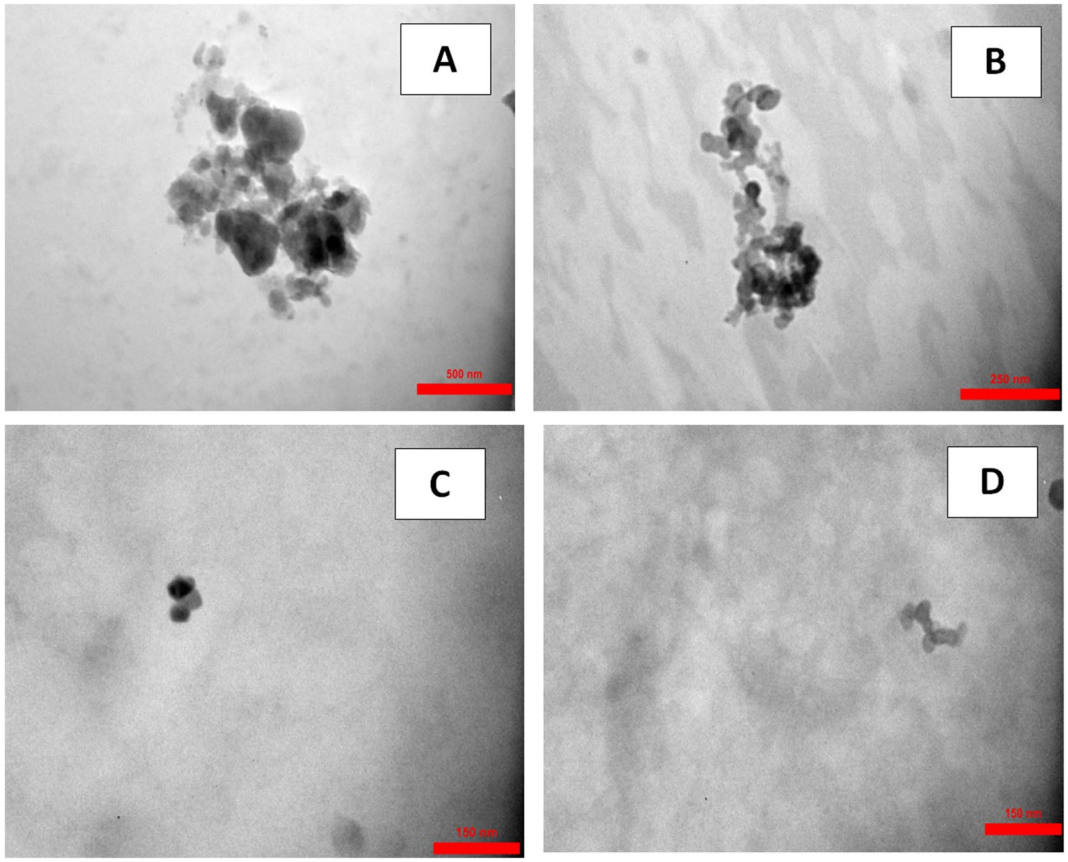

Fig. 2 Transmission electron microscopy images of the bulk clay (**A**) and nanoclay (**B**, **C**, and **D**)

the effective separation of nanoclay. This is also in agreement with the nanoclay particle size analysis obtained by TEM image analysis. The bulk clay size ranged from 806 to 2101 nm.

Specific surface area (SSA) and porosity analysis

The SSA, pore volume, and pore size distribution of the bulk clay and nanoclay are shown in Table 2. The nanoclay (111.9 $m^2\ g^{-1}$) had a much higher SSA than bulk clay (67.9 $m^2\ g^{-1}$). The SSA of the bulk clay is reported to have similar values with a smectite clay (61–66 $m^2\ g^{-1}$) using the N_2 gas adsorption measurement method (El Miz et al., 2017; Macht et al., 2011) which measures only external surface area of clays. The SSA obtained for smectite was in accordance with those reported by the other investigators and felt within their reported wide ranges of 50 to 130 $m^2\ g^{-1}$ (Kaufhold et al., 2010; Macht et al., 2011). The average pore diameter of bulk clay and nanoclay were 8.473 and 5.637 nm, respectively. According to the International Union of Pure and Applied Chemistry (IUPAC) classification, pore size is divided into three categories: macropores (> 50 nm), mesopores 2–50 nm, and micropores < 2 nm. As a result, bulk clay and nanoclay were in the range of mesopore size. The pore size results of this study are consistent with those of previous studies. Tarekegn et al. (2022) reported average pore sizes of 2.81 and 3.83 nm for nanoclay and iron-impregnated nanoclay, respectively, placing them in the mesopores category. Based on the BJH analysis results, the average nanopore diameter of bulk clay and nanoclay was 1.21 nm, and the total pore volume of bulk clay and nanoclay was 0.1437 and 0.1576 $cm^3\ g^{-1}$, respectively. The nitrogen (N_2) adsorption–desorption isotherm of the extracted bulk clay and nanoclay at 77 K is shown in Fig. 4. It

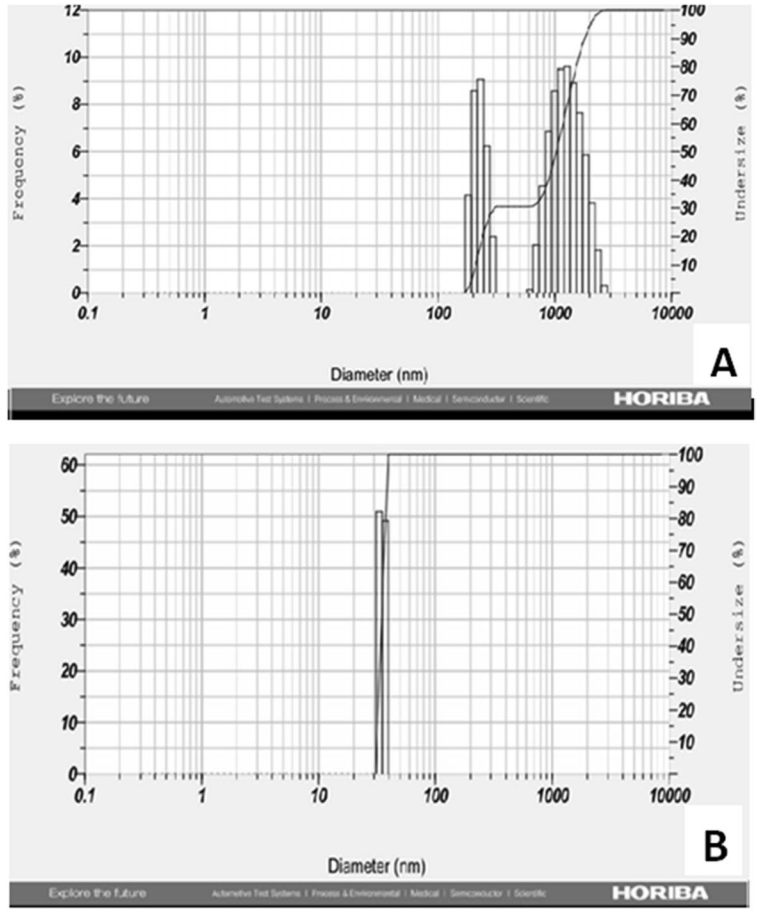

Fig. 3 Dynamic light scattering (DLS) images of (**A**) bulk clay and (**B**) nanoclay

Table 2 Specific surface area, volume, and pore size of extracted clay and nanoclay particles determined by BET and BJH analysis

Sample	BET plot			BJH plot
	The specific surface area, α_s BET (m^2g^{-1})	Total pore volume p/p_0 = 0.990 (cm^3g^{-1})	Mean pore diameter (nm)	Average nanopore diameter(nm)
Clay	67.86	0.1437	8.473	1.21
Nanoclay	111.85	0.1576	5.638	1.21

is clear from Fig. 4 that in the vapor pressure range below 0.1, the amount of N_2 adsorption in nanoclay (Fig. 4B) was higher than that of bulk clay. This is attributed to the higher proportion of micropores (high energy binding sites) in the nanoclay than that of bulk clay. As an energetic binding site, micropores are filled before other pores at very low pressure (Lowell et al., 2006). Researchers found that nanoclay adsorbs more N_2 than iron-saturated nanoclay at very low relative pressure (Tarekegn et al., 2022). At low relative pressures, a lower content of adsorbed N_2 (Fig. 4A) indicates the presence of mesopores in the absorbent structure (Geroeeyan et al., 2021). According to the IUPAC classification system, the bulk clay and nanoclay had the properties of type III isotherm and hysteresis loop H_3. The type of H_3 hysteresis loop of bulk clay and nanoclay is typically related to non-hard particles and plate-like particles (e.g., clays) (Geroeeyan et al., 2021; Khajeh & Ghaemi, 2019).

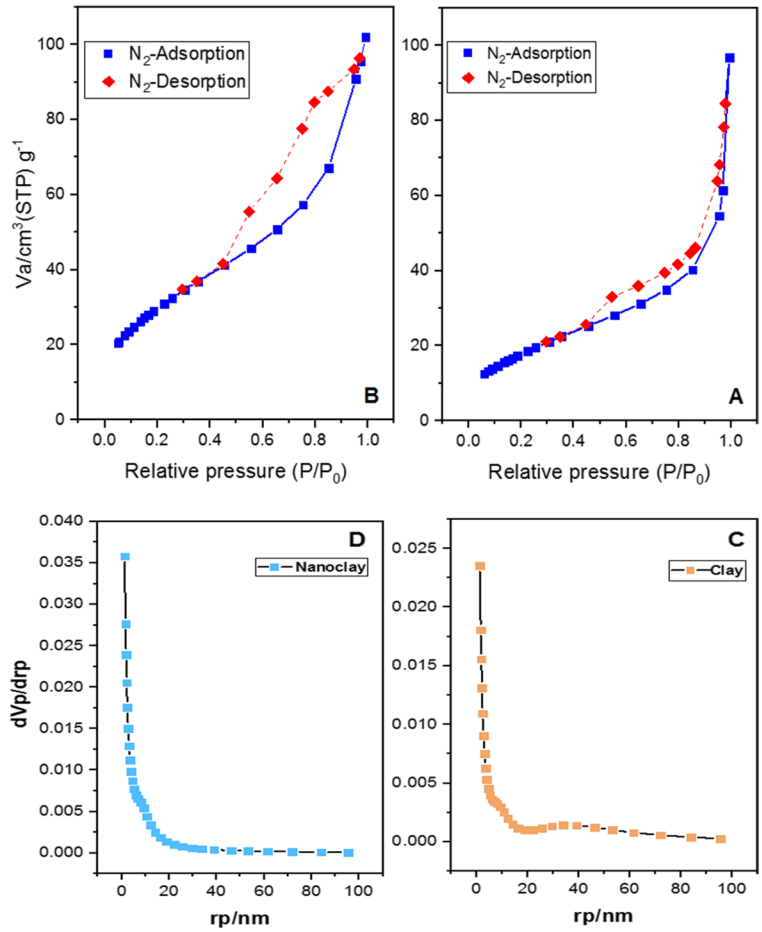

Fig. 4 Nitrogen adsorption–desorption isotherms of (**A**) bulk clay and (**B**) nanoclay and the BJH pore size distribution plot of extracted (**C**) bulk clay and (**D**) nanoclay

Total C analysis and pyrolysis GC–MS analysis

The total C content of clay and nanoclay fraction before and after H_2O_2 treatment is shown in Fig. 5. The C content of the clay before H_2O_2 treatment was 1.3 and that of the nanoclay was 1.6 (wt%). This indicates that the C content by mass in nanoclay was 1.2 times higher than that of bulk clay. Calabi-Floody et al. (2015) found that Andisol nanoclay contained 1.8–2.0 times more C than the bulk clay, while the Cambisol nanoclay contained 2.8–3.0 times more C than the bulk clay. Observed differences between the studies are likely due to differences in clay mineralogy, land use and climate.

After peroxide treatment, the C content of the clay fraction was reported to be 0.58 wt%, suggesting that chemical oxidation had a significant effect on the reduction of C content. In the nanoclay fraction, chemical oxidation caused a significant decrease

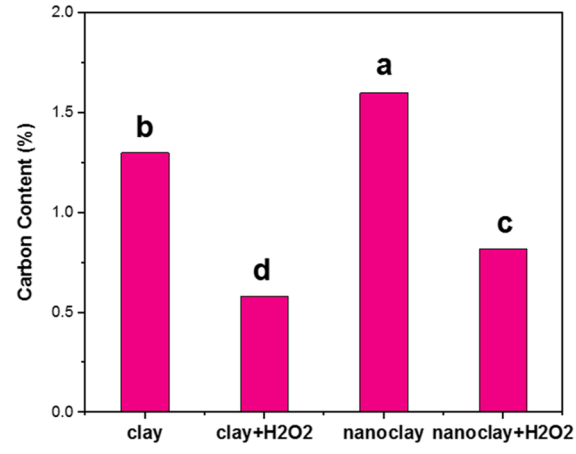

Fig. 5 Total C content of the extracted clay and nanoclay before and after treatment with H_2O_2. Treatments followed by a letter are not significantly different with a probability of error of 5% in Duncan's test

(0.82 wt%) in C content, which implies a 1.4 times enrichment factor in peroxide-resistant C in the nanoclay compared to the bulk clay. Thus, the SOC associated with the nanoclay was more resistant to chemical oxidation than the bulk soil clay. Calabi-Floody et al. (2015) reported a peroxide-resistant C enrichment factor of 1.3–2.6 times for Andisol nanoclay compared to bulk clay, and 2.2–2.6 times for Cambisol nanoclay compared to bulk clays.

The quantified compositions of the pyrolysis products of the bulk and nanoclays are shown in Fig. 6. Aromatic, organosilicon, N-containing compounds, hydrocarbons, isoprenoids, and carboxylic acid were identified in bulk clay and nanoclay. Before H_2O_2 treatment, aromatic compounds had a high relative abundance (more than 90%) in bulk clay and nanoclay, which agrees with the results of Wattel-Koekkoek et al. (2001). They found that the pyrolysis of SOM associated with smectite was rich in aromatic and phenolic compounds. It has also been previously shown that Vertisols have a high content of N-containing compounds, which consist of pyrrole, pyridine, and indole functional groups (Leinweber & Schulten, 1999). After H_2O_2 treatment, there was a substantial enrichment of the clay and nanoclay with N-containing functional groups and isoprenoids (Fig. 6). However, the H_2O_2-treated nanoclay had a much higher content of N-containing compounds (45%) than the H_2O_2-treated bulk clay (30%) fraction. A lower extent of removal of N-containing organic matter compared to C against H_2O_2 treatment

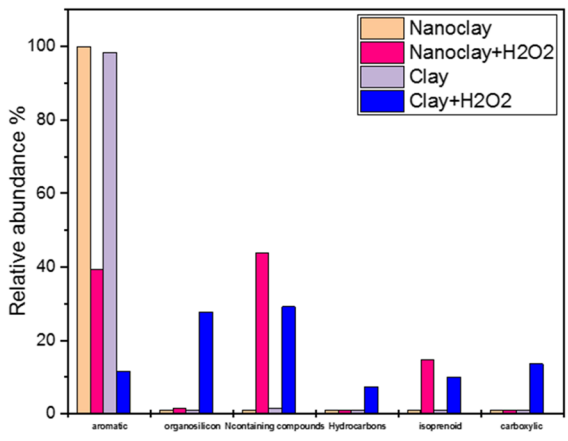

Fig. 6 Relative abundance of pyrolysis products identified by GC–MS of the extracted clay and nanoclay before and after treatment with H_2O_2

is the result of protection in microaggregates and the stronger interaction of N with the mineral surface (Helfrich et al., 2007).

Fourier-transform infrared (FTIR) spectroscopy

The FTIR spectra of clay and nanoclay fractions before and after treatment with H_2O_2 are shown in Fig. 7. In both spectra of the clay and nanoclay fractions, distinct absorption bands at the range of 3616 to 3696 cm^{-1} were observed, representing the stretching vibration of hydroxyl groups associated with clay minerals and quartz (Peltre et al., 2014). A broad band was observed at 3383–3388 cm^{-1}, which was attributed to the hydroxyl group (-OH) of several compounds such as phenol, alcohol, and carboxylic acid and N–H vibrations of amides and amides (Baumann et al., 2016; Bornemann et al., 2010; Peltre et al., 2014). The observed peaks at wave numbers 910 and 990 cm^{-1} indicate vibrational stretching of Al–OH and Si–O associated with the presence of layer silicate clay minerals such as kaolinite and smectite. Peaks at 700 and 800 cm^{-1} represent quartz (Borges et al., 2015; Churchman et al., 2010; Pacuła et al., 2006; Peltre et al., 2014). SOM consists of polyaromatic, aliphatic acids, amines, esters, and sugars. The interaction of these functional groups leads to the formation of broad peaks near 1600 and 1400 cm^{-1} (Nguyen et al., 1991). The observed peaks at 1600–1650 cm^{-1} indicated C=C stretching vibration and asymmetric stretching of -COO in ketones, carboxyl, and lignin (Bartos et al., 2020; Demyan et al., 2012; Margenot et al., 2017).

The spectra of the clay and nanoclay before treatment with H_2O_2 are similar. However, in the bulk clay sample (Fig. 7A), the adsorption peak at 1362 cm^{-1}, which represents the symmetric vibrations of carboxylate ions, was removed after treatment with H_2O_2, whereas the peak at 1380 cm^{-1} in the nanoclay fraction spectrum was still visible after H_2O_2 treatment, indicating that nanoclay lost less carboxylate organic matter than the clay. Similarly, the carboxyl group peak at 1632 cm^{-1} decreased in intensity to a greater extent in the clay compared to the nanoclay after H_2O_2 treatment. Thus, the absorption bands due to organic matter were less affected by peroxide treatment in the nanoclay than in the bulk clay sample (Calabi-Floody et al., 2011), which is in agreement with the total C results.

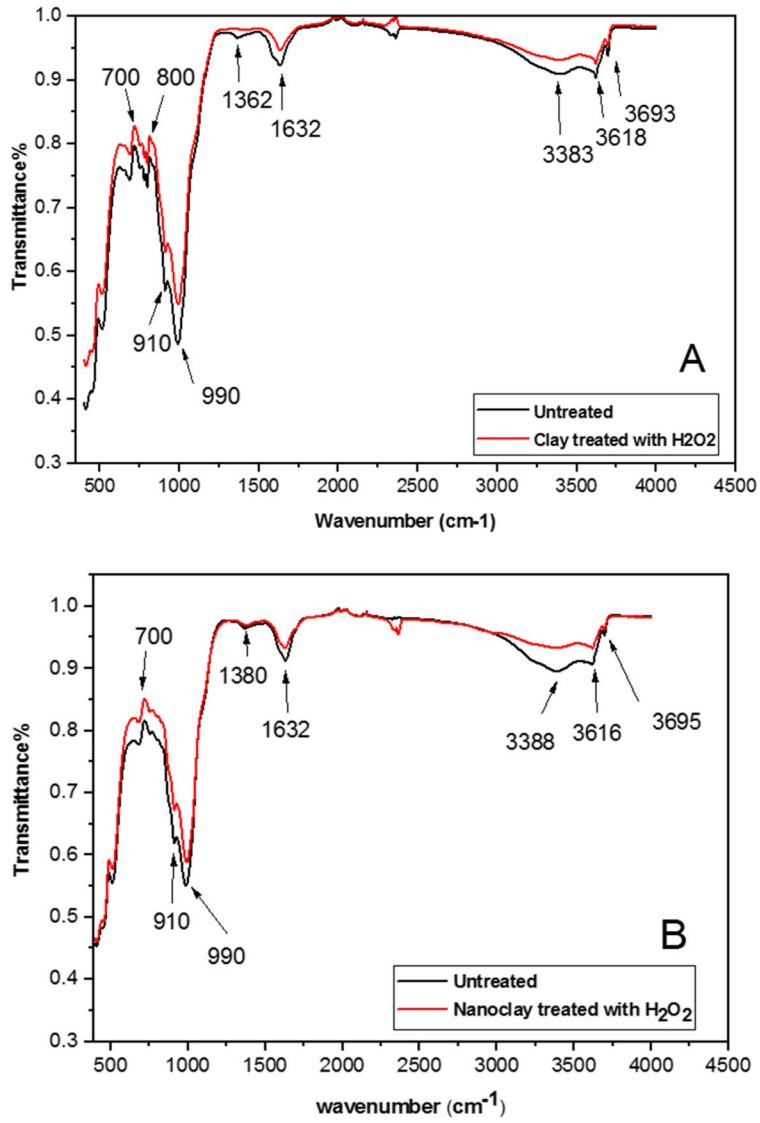

Fig. 7 Fourier-transform IR spectra of the bulk clay (**A**) and nanoclay (**B**) before and after treatment with H_2O_2

SEM results

Morphological characteristics of clay and nanoclay fractions before and after treatment with H_2O_2 obtained by scanning electron microscopy (SEM) are shown in Fig. 8. Based on the SEM images (Fig. 8C), the aggregates of the nanoclay fraction were smaller and more porous than that of the bulk clay fraction, which implies greater absorption of soil solution (Calabi-Floody et al., 2011; Okada et al., 2008). Before peroxide treatment, the clay and nanoclay aggregates have a simpler shape with smoother surfaces and edges. However, after peroxide treatment, the oxidation of organic matter resulted in a more irregular and uneven surface morphology, and a decrease in the number of aggregates and mesopore volume (Fig. 8B and 8D) (Brodowski et al., 2005; Falster et al., 2018; Li et al., 2019; Suazo-Hernández et al., 2021). Calabi-Floody et al. (2011) also reported that peroxide treatment of Andisol clay and nanoclay fractions resulted in more distinct shapes and boundaries, attributed to the oxidation of organic matter.

Zeta potential

The plot of the zeta potential of clay and nanoclay before and after treatment with H_2O_2 over a pH range of 2 to 8 is shown in Fig. 9. The zeta

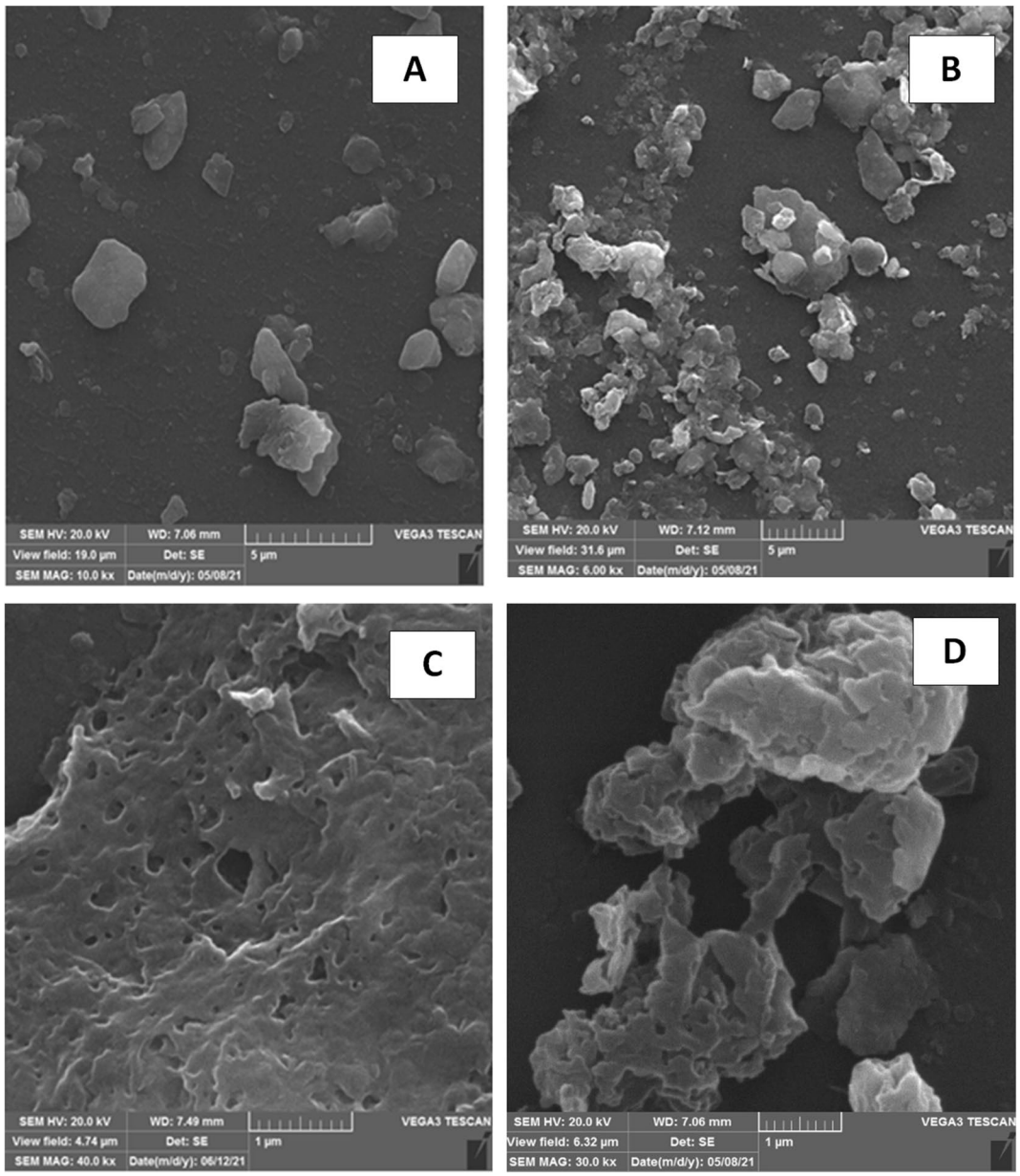

Fig. 8 Scanning electron micrographs sequence of (**A**) untreated and (**B**) H_2O_2- treated bulk clay, and (**C**) untreated and (**D**) H_2O_2 -treated nanoclay

potential value decreased to more negative values as the pH of the suspension increased. The negative zeta potential of clay minerals and organic matter increases with increasing pH, due to the deprotonation of mineral edge and acidic organic groups producing greater negative charge. High organic matter content increases negative charge, resulting in a more negative soil zeta potential (Marchuk et al., 2013). After treatment with H_2O_2, the zeta potential was observed to decrease in both fractions due to the oxidation of organic matter, but to a greater extent in the bulk clay fraction (Fig. 9A). Peroxide treatment increased the isoelectric point (IEP) of the clay from 2.2 to 3.3 (Fig. 9A) and of the nanoclay from 2.0 to 2.2 (Fig. 9B). The lower IEP of the peroxide-treated nanoclay compared to the bulk clay indicates

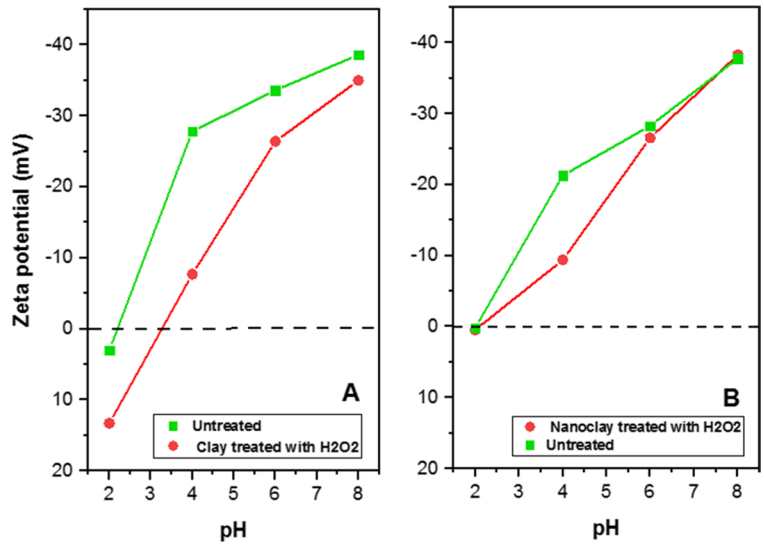

Fig. 9 Zeta potentials as a function of suspension pH for (**A**) bulk clay before and after treatment with H_2O_2; and (**B**) nanoclay before and after treatment with H_2O_2

a relatively higher content of organic matter (Calabi-Floody et al., 2011). The lower IEP of the peroxide-treated nanoclay also indicates greater chemical stabilization of the organic matter in the nanoclay with a higher surface area (Calabi-Floody et al., 2015). Clay minerals with high specific surface area and expanding layers, such as smectite and vermiculite, have a high affinity for carbohydrates and aliphatic organic matter and have the most important organic matter stabilizing ability (Dong et al., 2018; Loehr & Kennedy, 2014). The uncharged microsites of smectites can adsorb nonpolar or uncharged organic groups (e.g., alkyl-C and aromatic groups) by Van Der Waals forces (Sarkar et al., 2018).

Conclusions

The nanoclay extracted from the Vertisol was dominated by 2:1 layer silicates and had an estimated particle size between 16 and 46 nm. It had a much greater surface area which was more porous than the bulk clay. The nanoclay contained 1.2 times the C content of the bulk clay prior to peroxide treatment. However, the nanoclay was enriched with 1.4 times more C than the bulk clay after peroxide treatment, indicating that SOC was more stabilized in the nanoclay. This was also confirmed by the FTIR and zeta potential results. About 45% of the resistant organic material in the nanoclay was identified with N-containing compounds, indicating that these compounds contribute to organic C stability. The results demonstrate the important contribution of nanoclay in soil C sequestration in semi-arid Vertisols.

Acknowledgements The authors would like to appreciate Shiraz University for providing research facilities.

Author contribution NS: conceptualization, methodology, research, software, sources, formal analysis, manuscript writing. MB: monitoring, review, editing, and project management. RG-F and AAM: supervision and editing. AGH: manuscript editing.

Data availability The dataset analyzed or used in the present study is available from available from the corresponding author on reasonable request.

Declarations

Competing interests The authors declare no competing interests.

References

Ahmat, A. M., Boussafir, M., Milbeau, C. L., Guégan, R., Oliveira, T. D., & Forestier, L. L. (2017). Organic matter and clay interaction in a meromictic lake: Implications for source rock OM preservation (Lac Pavin, Puy-de-Dôme, France). *Organic Geochemistry, 109*, 47–57. https://doi.org/10.1016/j.orggeochem.2017.03.014

Angst, G., Mueller, K. E., Kögel-Knabner, I., Freeman, K. H., & Mueller, C. W. (2017). Aggregation controls the stability of lignin and lipids in clay-sized particulate and

mineral associated organic matter. *Biogeochemistry, 132*, 307–324. https://doi.org/10.1007/s10533-017-0304-2

Atigh, B. Q. Z., Heidari, A., Karimi, A., Pezhman, M. A., Lajayer, B. A., & Lima, E. C. (2021). Purification and economic analysis of nanoclay from bentonite. *Environmental Science and Pollution Research, 28*, 13690–13696. https://doi.org/10.1007/s11356-020-11595-1

Barrett, E. P., Joyner, L. G., & Halenda, H. P. (1951). The determination of pore volume and area distributions in porous substance. I. Computations from nitrogen isotherms. *Jornula of the American Chemical Society, 73*, 373–380. https://doi.org/10.1021/ja01145a126

Bartos, A., Szyma'nski, W., & Klimek, M. (2020). Impact of conventional agriculture on the concentration and quality of water-extractable organic matter (WEOM) in the surface horizons of Retisols—A case study from the Carpathian foothills in Poland. *Soil and Tillage Research, 204*, 104750. https://doi.org/10.1016/j.still.2020.104750

Baumann, K., Schöning, I., Schrumpf, M., Ellerbrock, R. H., & Leinweber, P. (2016). Rapid assessment of soil organic matter: Soil color analysis and Fourier transform infrared spectroscopy. *Geoderma, 278*, 49–57. https://doi.org/10.1016/j.geoderma.2016.05.012

Blum, W. E. H., & Eswaran, H. (2004). Soils for sustaining global food production. *Jornula of Food Science, 69*, 37–42. https://doi.org/10.1111/j.1365-2621.2004.tb15490.x

Borges, R., Brunatto, S. F., Leitão, A. A., de Carvalho, G. S. G., & Wypych, F. (2015). Solid-state mechanochemical activation of clay minerals and soluble phosphate mixtures to obtain slow-release fertilizers. *Clay Minerals, 50*, 153–162. https://doi.org/10.1180/claymin.2015.050.2.0

Bornemann, L., Welp, G., & Amelung, W. (2010). Particulate organic matter at the field scale: Rapid acquisition using mid-infrared spectroscopy. *Soil Science Society of America Journal, 74*, 1147–1156. https://doi.org/10.2136/sssaj2009.0195

Brodowski, S., Amelung, W., Haumaier, L., Abetz, C., & Zech, W. (2005). Morphological and chemical properties of black carbon in physical soil fractions as revealed by scanning electron microscopy and energy-dispersive X-ray spectroscopy. *Geoderma, 128*, 116–129. https://doi.org/10.1016/j.geoderma.2004.12.019

Brunauer, S., Emmet, P. H., & Teller, E. (1938). Adsorption of gases in multimolecular layers. *Jornula of the American Chemical Society, 60*, 309–319. https://doi.org/10.1021/ja01269a023

Calabi-Floody, M., Theng, B. K. G., Reyes, P., & Mora, M. L. (2009). Natural nanoclays: Applications and future trends a Chilean perspective. *Clay Minerals, 44*, 161–176. https://doi.org/10.1180/claymin.2009.044.2.161

Calabi-Floody, M., Bendal, J. S., Jara, A. A., Welland, M. E., Theng, B. K. G., Rumpel, C., & Mora, M. D. L. (2011). Nanoclays from an Andisol: Extraction, properties and carbon stabilization. *Geoderma, 161*, 159–167. https://doi.org/10.1016/j.geoderma.2010.12.013

Calabi-Floody, M., Rumpel, C., Velásquez, G., Violante, A., Bol, R., Condron, L. M., & Mora, M. L. (2015). Role of Nanoclays in carbon stabilization in Andisols and Cambisols. *Journal of Soil Science and Plant Nutrition, 15*, 587–604. https://doi.org/10.4067/S0718-95162015005000026

Carbajal-de-la-Torre, G. (1998). Electron microscopy and X-ray analysis of lacustrine clays from the Charo Canyon, State of Michoacán, Mexico. *Clays and Clay Minerals, 46*, 330–339. https://doi.org/10.1346/CCMN.1998.046031 2

Chapman, H. D. (1965). Cation exchange capacity. In C. A. Black (Ed.), *Methods of soil analysis, part 2* (pp. 891–901). American Society of Agronomy.

Chen, S. L., Hong, H. L., Huang, X. Y., Fang, Q., Yin, K., Wang, C. W., Zhang, Y. M., Cheng, L. L., & Algeo, T. J. (2018). The role of organo-clay associations in limiting organic matter decay: Insights from the Dajiuhu peat soil, Central China. *Geoderma, 320*, 149–160. https://doi.org/10.1016/j.geoderma.2018.01.013

Churchman, G. J., Foster, R. C., D'Acqui, L. P., Janik, L. J., Skjemstad, J. O., Merry, R. H., & Weissmann, D. A. (2010). Effect of land-use history on the potential for carbon sequestration in an Alfisol. *Soil Tillage Research, 109*, 23–35. https://doi.org/10.1016/j.still.2010.03.012

Churchman, G. J., Singh, M., Schapel, A., Sarkar, B., & Bolan, N. (2020). Clay minerals as the key to the sequestration of carbon in soils. *Clays and Clay Minerals*, *68* (2). https://doi.org/10.1007/s42860-020-00071-z

Coulombe, C. E., Wilding, L. P., & Dixon, J. B. (1996). Overview of Vertisols: Characteristics and impacts on society. *Advances in Agronomy, 57*, 289–375. https://doi.org/10.1016/S0065-2113(08)60927-X

Das, A., Purakayastha, T. J., Ahmed, N., Das, R., Biswas, S., Singh Shivay, Y., Sehgal, V. K., Rani, K., Trivedi, A., Tigga, P., Sahoo, J., Chakraborty, R., & Sen, S. (2022). Influence of clay mineralogy on soil organic carbon stabilization under tropical climate, India. *Journal of Soil Science and Plant Nutrition, 23*, 1003–1018. https://doi.org/10.1007/s42729-022-01099-x

Demyan, M. S., Rasche, F., Schulz, E., Breulmann, M., Müller, T., & Cadisch, G. (2012). Use of specific peaks obtained by diffuse reflectance Fourier transform mid-infrared spectroscopy to study the composition of organic matter in a haplic Chernozem. *European Journal of Soil Science, 63*, 189–199. https://doi.org/10.1111/j.1365-2389.2011.01420.x

Dong, F., Guo, Y., Liu, M., Zhou, L., Zhou, Q., & Li, H. (2018). Spectroscopic evidence and molecular simulation investigation of the bonding interaction between lysine and montmorillonite: Implications for the distribution of soil organic nitrogen. *Applied Clay Science, 159*, 3–9. https://doi.org/10.1016/j.clay.2017.11.020

El Miz, M., Akichoh, H., Berraaouan, D., Salhi, S., & Tahani, A. (2017). Chemical and physical characterization of Moroccan bentonite taken from Nador (North of Morocco). *American Journal of Chemistry, 7*, 105–112. https://doi.org/10.5923/j.chemistry.20170704.01

Falster, G., Delean, S., & Tyler, J. (2018). Hydrogen peroxide treatment of natural lake sediment prior to carbon and oxygen stable isotope analysis of calcium carbonate, geochemistry, geophysics. *Geosystems, 19*, 3583–3595. https://doi.org/10.1029/2018GC007575

Feng, W., Plante, A. F., & Six, J. (2013). Improving estimates of maximal organic carbon stabilization by fine soil particles. *Biogeochemistry, 112*, 81–93. https://doi.org/10.1007/s10533-011-9679-7

Fesharaki, O., García-Romero, E., Cuevas-González, J., & López-Martínez, N. (2007). Clay mineral genesis and chemical evolution in the Miocene sediments of Somosaguas, Madrid Basin, Spain. *Clay Minerals, 42*, 187–201. https://doi.org/10.1180/claymin.2007.042.2.05

Francesca Cotrufo, M., & Lavallee, J. M. (2022). Soil organic matter formation, persistence, and functioning: A synthesis of current understanding to inform its conservation and regeneration. In D. Sparks, (Ed.), *Advances in Agronomy, Academic Press* (pp. 1–66). Elsevier BV. https://doi.org/10.1016/bs.agron.2021.11.002

Geroeeyan, A., Niazi, A., & Konoz, E. (2021). Removal of Basic Orange 2 dye and Ni^{2+} from aqueous solutions using alkaline-modified nanoclay. *Water Science and Technology, 83*, 2271–2286. https://doi.org/10.2166/wst.2021.121

Ghosh, S., Adsul, T., & Varma, A. K. (2023). Organic matter and mineralogical acumens in CO_2 sequestration. In D. Inamuddin, & T. Altalhi (Eds.) *Green Sustainable Process for Chemical and Environmental Engineering and Science* (pp. 561–594). Elsevier. ISBN: 9780323994309

Heidari, A., & Mahmoodi, S. H. (2005). Micromorphological characteristics of Vertisols of Iran, including nonsmectitic soils. *Arid Land Research and Management, 19*, 29–46. https://doi.org/10.1080/15324980590887164

Helfrich, M., Flessa, H., Mikutta, R., Dreves, A., & Ludwig, B. (2007). Comparison of chemical fractionations methods for isolating stable soil organic carbon pools. *European Journal of Soil Science, 58*, 1316–1329. https://doi.org/10.1111/j.1365-2389.2007.00926.x

Kaufhold, S., Dohrmann, R., Klinkenberg, M., Siegesmund, S., & Ufer, K. (2010). N_2-BET specific surface area of bentonites. *Journal of Colloid and Interface Science, 349*, 275–282. https://doi.org/10.1016/j.jcis.2010.05.018

Khajeh, M., & Ghaemi, A. (2019). Nanoclay montmorillonite as an adsorbent for CO_2 capture: Experimental and modeling. *Journal of the Chinese Chemical Society, 67*, 253–266. https://doi.org/10.1002/jccs.201900150

Kumar, R., Mangalapuri, R., Ahmadi, M. H., Dai-Viet, N. V., Solanki, R., & Kumar, P. (2020). The role of nanotechnology on post-combustion CO_2 absorption in process industries. *International Journal of Low-Carbon Technologies, 15*, 361–367. https://doi.org/10.1093/ijlct/ctaa002

Lal, R. (2015). Soil erosion and carbon dynamics. *Soil & Tillage Research, 81*, 137–142. https://doi.org/10.1016/j.still.2004.09.002

Leinweber, P., & Schulten, H. R. (1999). Advances in analytical pyrolysis of soil organic matter. *Journal of Analytical and Applied Pyrolysis, 49*, 359–383. https://doi.org/10.1016/S0165-2370(98)00082-5

Li, B., Li, H., Wei, Y., Zhang, X., Wei, D., & Li, J. (2019). Microscopic properties of hydrogen peroxide activated crumb rubber and its influence on the rheological properties of crumb rubber modified asphalt. *Materials, 12*, 1434. https://doi.org/10.3390/ma12091434

Loehr, S. C., & Kennedy, M. J. (2014). Organomineral nanocomposite carbon burial during Oceanic Anoxic Event 2. *Biogeosciences, 11*, 4971–4983. https://doi.org/10.5194/bg-11-4971-2014

Lowell, S., Shields, J. E., Thomas, M. A., & Thommes, M. (2006). Characterization of porous solids and powders: Surface area, pore size and density. *Springer*. https://doi.org/10.1007/978-1-4020-2303-3

Lützow, M. V., Kögel-Knabner, A. I., Ekschmitt, A. K., Matzner, B. E., Guggenberger, C. G., Marschner, D. B., & Flessa, F. E. H. (2006). Stabilization of organic matter in temperate soils: Mechanisms and their relevance under different soil conditions – A review. *European Journal of Soil Science, 57*, 426–445. https://doi.org/10.1111/j.1365-2389.2006.00809.x

Macht, F., Eusterhues, K., Pronk, G. J., & Totsche, K. U. (2011). Specific surface area of minerals: Comparison between atomic force microscopy measurements and bulk-gas (N_2) and -liquid (EGME) adsorption methods. *Applied Clay Science, 53*, 20–26. https://doi.org/10.1016/j.clay.2011.04.006

Marchuk, A., Rengasamy, P., & McNeill, A. (2013). Influence of organic matter, clay mineralogy, and pH on the effects of CROSS on soil structure is related to the zeta potential of the dispersed clay. *Soil Research, 51*, 34–40. https://doi.org/10.1071/SR13012

Margenot, A. J., Calder'on, F. J., Goyne, K. W., Mukome, F. N. D., & Parikh, S. J. (2017). IR spectroscopy, soil analysis applications. *Encyclopedia of Spectroscopy and Spectrometry, 3*, 448–454. https://doi.org/10.1016/B978-0-12-409547-2.12170-5

Mehra, O. P., & Jackson, M. L. (1958). Iron oxide removal from soils and clays by dithionate citrate system with sodium bicarbonate. *Clays and Clay Minerals, 7*, 317–327. https://doi.org/10.1016/B978-0-08-009235-5.50026-7

Mehrabadi, Z., & Faghihian, H. (2018). Comparative photocatalytic performance of TiO2 supported on clinoptilolite and TiO2/Salicylaldehyde-NH2-MIL-101(Cr) for degradation of pharmaceutical pollutant atenolol under UV and visible irradiations. *Journal of Photochemistry and Photobiology A: Chemistry, 102–111*,. https://doi.org/10.1016/j.jphotochem.2017.12.042

Minasny, B., Malone, B. P., McBratney, A. B., Angers, D. A., Arrouays, D., Chambers, A., Chaplot, V., Chen, Z. S., Cheng, K., Das, B. S., Field, D. J., Gimona, A., Hedley, C. B., Hong, S. Y., Mandal, B., Marchant, B. P., Martin, M., McConkey, B. G., Mulder, V. L., … Winowiecki, L. (2017). Soil carbon 4 per mille. *Geoderma, 292*, 59–86. https://doi.org/10.1016/j.geoderma.2017.01.002

Monreal, C. M., Sultan, Y., & Schnitzer, M. (2010). Soil organic matter in nano-scale structures of a cultivated Black Chernozem. *Geoderma, 159*, 237–242. https://doi.org/10.1016/j.geoderma.2010.07.017

Najafi Ghiri, M., & Abtahi, A. (2011). Potassium dynamics in calcareous Vertisols of southern Iran. *Arid Land Research and Management, 25*, 257–274. https://doi.org/10.1080/15324982.2011.565857

Nelson, D. W., & Sommers, L. E. (1982). Total carbon, organic carbon, and organic matter. In A. L. Page (Ed.), *Methods of soil analysis, part 2* (pp. 539–579). American Society of Agronomy.

Nguyen, T. T., Janik, L. J., & Raupach, M. (1991). Diffuse reflectance infrared Fourier transform (DRIFT) spectroscopy in soil studies. *Australian Journal of Soil Research, 29*, 49–67. https://doi.org/10.1071/SR9910049

Okada, K., Matsui, S., Isobe, T., Kameshima, Y., & Nakajima, A. (2008). Water-retention properties of porous ceramics prepared from mixtures of allophane and vermiculite for materials to counteract heat island effects. *Ceramics International, 34*, 345–350. https://doi.org/10.1016/j.ceramint.2006.10.006

Pacuła, A., Bielanska, E., Gaweł, A., Bahranowski, K., & Serwicka, E. M. (2006). Textural effects in powdered montmorillonite induced by freeze-drying and ultrasound pretreatment. *Applied Clay Science, 32*, 64–72. https://doi.org/10.1016/j.clay.2005.10.002

Pal, D. K., Wani, S. P., & Sahrawat, K. L. (2012). Vertisols of tropical Indian environments: Pedology and edaphology. *Geoderma, 189–190*, 28–49. https://doi.org/10.1016/j.geoderma.2012.04.021

Paul, R., Datta, S. C., Manjaiah, K. M., & Bhattacharyya, R. (2017). X-ray crystallinity of different soil nanoclays in relation to phosphatase adsorption. *Applied Clay Science, 144*, 19–25. https://doi.org/10.1016/j.clay.2017.05.002

Paul, R., Kaunakaran, K., Vasu, D., Tiwary, P., & Chandran, P. (2021). Origin and mineralogy of nano clays of Indian Vertisols and their implications in selected soil properties. *Eurasian Soil Science, 54*, 572–585. https://doi.org/10.1134/S1064229321040128

Paustian, K., Larson, E., Kent, J., Marx, E., & Swan, A. (2019). Soil C sequestration as a biological negative emission strategy. *Frontiers in Climate*. https://doi.org/10.3389/fclim.2019.00008

Peltre, C., Bruun, S., Du, C., Thomsen, Ik., & Jensen, L. S. (2014). Assessing soil constituents and labile soil organic carbon by mid-infrared photoacoustic spectroscopy. *Soil Biology and Biochemistry, 77*, 41–50. https://doi.org/10.1016/j.soilbio.2014.06.022

Powlson, D. S., Whitmore, A. P., & Goulding, K. W. T. (2011). Soil carbon sequestration to mitigate climate change: A critical reexamination to identify the true and the false. *European Journal of Soil Science, 62*, 42–55. https://doi.org/10.1111/j.1365-2389.2010.01342.x

Pramanik, P., Ray, P., Maity, A., Das, S., Ramakrishnan, S., & Dixit, P. (2020). *Nanotechnology for improved carbon management in soil*. Springer, Singapore: Carbon Management in Tropical and Sub-Tropical Terrestrial Systems.

Rowell, D. L. (1994). *Soil science: Methods and applications*. Longman Scientific and Technical: London, UK.

Salinity Laboratory Staff. (1954). *Diagnosis and improvement of saline and alkali soils. Handbook No. 60.* United States Department of Agriculture, Washington, DC.

Sarkar, B., Singh, M., Mandal, S., Churchman, G. J., & Bolan, N. S. (2018). Clay minerals organic matter interactions in relation to carbon stabilization in soils. In C. Garcia, P. Nannipieri, & T. Hernandez (Eds.), *The Future of Soil Carbon Its Conservation and Formation* (pp. 71–86). Academic Press.

Schrumpf, M., Kaiser, K., Guggenberger, G., Persson, T., Kögel-Knabner, I., & Schulze, E. D. (2013). Storage and stability of organic carbon in soils as related to depth, occlusion within aggregates, and attachment to minerals. *Biogeosciences, 10*, 1675–1691. https://doi.org/10.5194/bg-10-1675-2013

Singh, M., Sarkar, B., Sarkar, S., Churchman, J., Bolan, N., Mandal, S., Menon, M., Purakayastha, T. J., & Beerling, D. J. (2018). Stabilization of soil organic carbon as influenced by clay mineralogy. *Advances in Agronomy, 148*, 33–84. https://doi.org/10.1016/bs.agron.2017.11.001

Six, J., Conant, R. T., Paul, E. A., & Paustian, K. (2002). Stabilization mechanisms of soil organic matter: Implications for C-saturation of soils. *Plant and Soil, 241*, 155–176. https://doi.org/10.1023/A:1016125726789

Suazo-Hernández, J., Klumpp, E., Arancibia-Miranda, N., Poblete-Grant, P., Jara, A., Bol, R., & Luz Mora, M. L. (2021). Describing phosphorus sorption processes on volcanic soil in the presence of copper or silver engineered nanoparticles. *Materials, 11*, 373. https://doi.org/10.3390/min11040373

Tarekegn, M. M., Balakrishnan, R. M., Hiruy, A., Hussen, A., & Maanyam, H. S. (2022). Nano-clay and iron impregnated clay nanocomposite for Cu^{2+} and Pb^{2+} ions removal from aqueous solutions. *Air, Soil and Water Research, 15*, 118. https://doi.org/10.1177/11786221221094037

Wattel-Koekkoek, E. J. W., van Genuchten, P. P. L., Buurman, P., & van Lagen, B. (2001). Amount and composition of clay-associated soil organic matter in a range of kaolinitic and smectitic soils. *Geoderma, 99*, 27–49. https://doi.org/10.1016/S0016-7061(00)00062-8

Whittig, L. D., & Allardice, W. R. (1986). X-ray diffraction techniques, Methods of Soil Analysis, Part 1: Physical and Mineralogical Methods. In A. Klute, (Ed.), American *Society of Agronomy, Madison* (pp. 331-362). https://doi.org/10.2136/sssabookser5.1.2ed

Yang, Y., Shen, Z., Bissett, A., & Viscarra Rossel, R. (2021). Estimating soil fungal abundance and diversity at a macroecological scale with deep learning spectrotransfer functions. *The Soil, 8*, 223–235. https://doi.org/10.5194/soil-8-223-2022

Zayed, A. M., Wahed, M. S. A., Mohamed, E. A., & Sillanpää, M. (2018). Insights on the role of organic matters of some Egyptian clays in methyl orange adsorption: Isotherm and kinetic studies. *Applied Clay Science, 166*, 49–60. https://doi.org/10.1016/j.clay.2018.09.013